Trap pumping schemes for the Euclid CCD273 detector: characterisation of electrodes and defects

Journal Item

For guidance on citations see FAQs.

oro.open.ac.uk

Trap pumping schemes for the Euclid CCD273 detector: Characterisation of electrodes and defects

Jesper Skottfelt,[a,1] **David J. Hall,**[a] **Ben Dryer,**[a] **Nathan Bush,**[a] **Julia Campa,**[a] **Jason P. D. Gow,**[a,2]
Andrew D. Holland,[a] **Douglas Jordan,**[b] **David Burt**[b]

[a]*Centre for Electronic Imaging, Open University, Walton Hall, Milton Keynes, MK7 6AA, UK*
[b]*Teledyne e2v, 106 Waterhouse Lane, Chelmsford, Essex, CM1 2QU, UK*

E-mail: jesper.skottfelt@open.ac.uk

ABSTRACT: The VISible imager instrument (VIS) on board the Euclid mission will deliver high resolution shape measurements of galaxies down to very faint limits ($R \sim 25$ at 10σ) in a large part of the sky, in order to infer the distribution of dark matter in the Universe. To help mitigate radiation damage effects that will accumulate in the detectors over the mission lifetime, the properties of the radiation induced traps needs to be known with as high precision as possible. For this purpose the trap pumping method will be employed as part of the in-orbit calibration routines. Using trap pumping it is possible to identify and characterise single traps in a Charge-Coupled Device (CCD), thus providing information such as the density, emission time constants and sub-pixel positions etc. of the traps in the detectors.

This paper presents the trap pumping algorithms used for the radiation testing campaign of the CCD273 detectors, performed by the Centre for Electronic Imaging (CEI) at the Open University, that will be used for the VIS instrument. The CCD273 is a four-phase device with uneven phase widths, which complicates the trap pumping analysis. However, we find that by optimising the trap pumping algorithms and analysis routines, it is possible to obtain sub-pixel and even sub-phase positional information about the traps. Further, by comparing trap pumping data with simulations, it is possible to gain more information about the effective electrode widths of the device.

KEYWORDS: Detectors for UV, visible and IR photons; Data analysis; Space instrumentation; Detector modelling and simulations II

---

¹Corresponding author.
²Now at Mullard Space Science Laboratory, University College London, Holmbury St Mary, Dorking, Surrey RH5 6NT, UK

Contents

1   Introduction

The scientific aim of the Euclid mission [1], the second medium-class mission in the Cosmic Vision programme of the European Space Agency, is to map the geometry of the Dark Universe. For this purpose two instruments will be used; the Visible Imager (VIS) [2] and the Near Infrared Photometer Spectrometer (NISP) [3]. Using a large focal plane, 36 4K×4K Charge-Coupled Devices (CCDs), the VIS instrument will do large scale observations to enable Weak Lensing measurements. By measuring the ellipticity of the galaxies in a large part of the extra-galactic sky, it is possible to infer the mass distribution of the matter that distorts the galaxy shapes and thereby map the dark matter. In order for this experiment to be successful, the point spread function has to be very stable and tightly controlled and a very deep understanding of the systematic effects are therefore needed.

An important systematic effect comes from the degrading of the detectors in the harsh radiation environment outside the Earth's atmosphere. Highly energetic particles, mainly generated by the Sun, are able to penetrate the silicon lattice of a CCD and displace silicon atoms. This creates vacancies that can act as traps for electrons. During readout of the CCD the traps can capture electrons and release then at a later point in time, thus creating smearing that will have a detrimental effect on the galaxy shape measurements unless corrected for to a very high precision.

As the radiation damage will increase over the mission lifetime, it is important that the density of traps can be tracked while Euclid is in space. However, to reach the required level of radiation damage correction for the Euclid VIS instrument, more information than just the density of traps is needed [4, 5].

Using the trap pumping method [6–10] it is possible to identify and characterise single traps. This can give information about several trap parameters, such as emission time constant, capture probability, sub-pixel position, energy levels and emission cross section. The trap pumping technique has therefore been implemented as a part of the available in-orbit calibration routines for the Euclid VIS instrument [2].

2   Trap pumping theory

Trap pumping is performed by moving, or clocking, charge between the electrodes of the CCD in a specific pattern and at a fixed phase time (t_{ph}). For a three-phase device with even-sized electrodes, the normal way to clock the device for trap pumping is to move the charge between phases 1-2-3-1'-3-2-1, where 1' denotes phase 1 in the adjacent pixel (see figure 1). If a trap is present under phase 2 it will be able to capture an

electron when the charge packet is in that phase (second panel of figure 1). If the trap releases the electron between t_{ph} and $2t_{ph}$ (forth panel of figure 1) it will join the charge packet of the adjacent pixel. This means that if the phase time resonates with the emission time constant (τ_e) of the trap, charge will effectively be shuffled from one pixel to the next. If this clocking pattern, or clocking scheme, is repeated a number (N) times, a dipole will be formed as shown in figure 2.
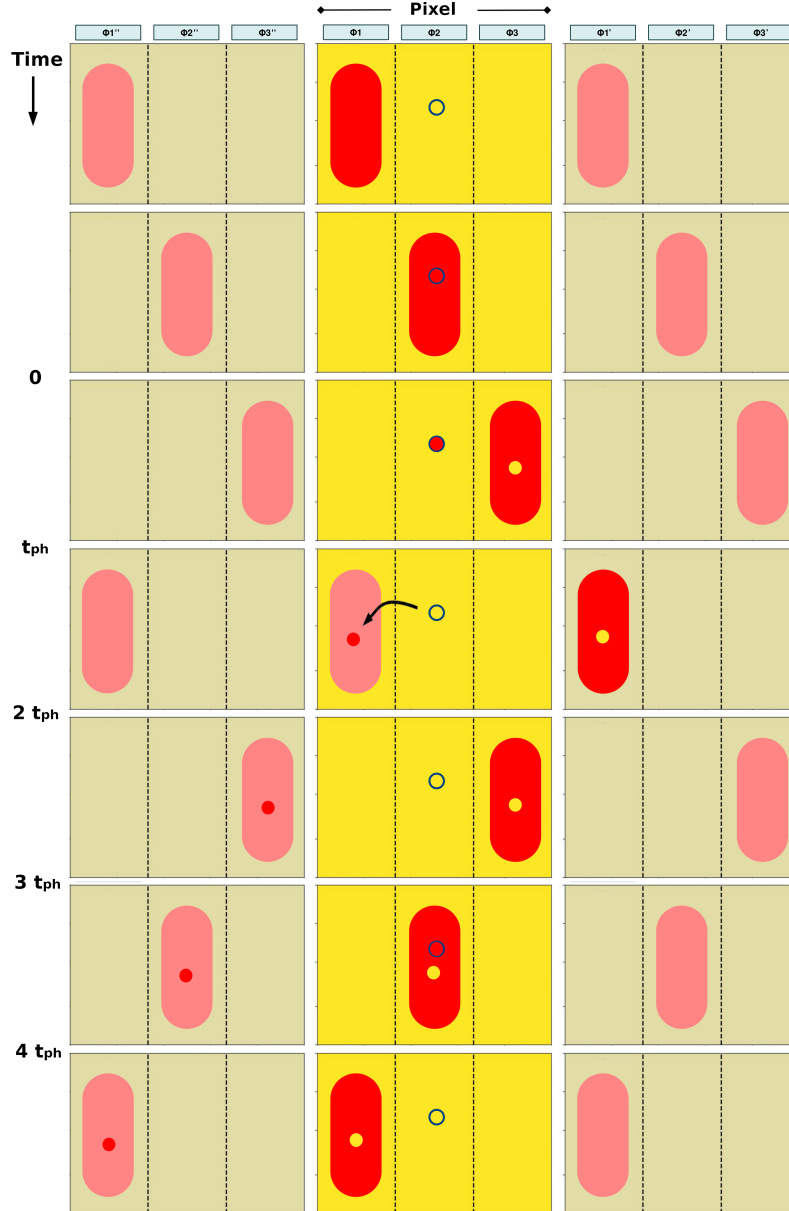
Figure 1. Standard trap pumping clocking scheme for 3 phase device. Trap is moved from phases 1-2-3-1'-3-2-1. If a trap is present under phase 2 it can capture an electron, and if that electron is released between t_{ph} and $2t_{ph}$, it will be moved to the charge packet in the adjacent pixel.

The same is true for a trap under phase 3, but in this case the charge will be shuffled in the other direction, and the dipole will therefore have the opposite direction. Traps under phase 1 will be able to capture charge from two different charge packets and any significant dipole will therefore not form. To detect traps under
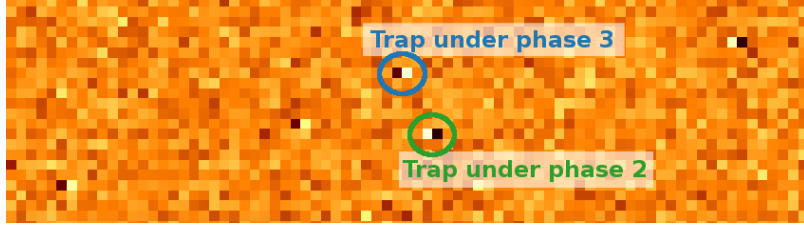
Figure 2. Example of dipoles from laboratory data. Indicated are the direction of dipoles from a trap under phase 2 (high-low) and phase 3 (low-high) using the standard three-phase clocking scheme.

phase 1 the starting point of the clocking scheme would need to be moved, for instance to 2-3-1'-2'-1'-3-2 in which case traps under phase 3 and 1 can be detected.

The intensity of the dipole is given by

$$I = NP_c \left[\exp\left(\frac{-t_{ph}}{\tau_e}\right) - \left(\frac{-2t_{ph}}{\tau_e}\right) \right], \tag{2.1}$$

where P_c is the probability of capture [10]. By running the clocking scheme at a range of t_{ph} values, the trap will give different dipole intensities (see figure 3 lower panel). If these intensities are fitted with eq. 2.1 it is possible to extract τ_e and P_c of the trap, as shown in figure 3 (upper panel).
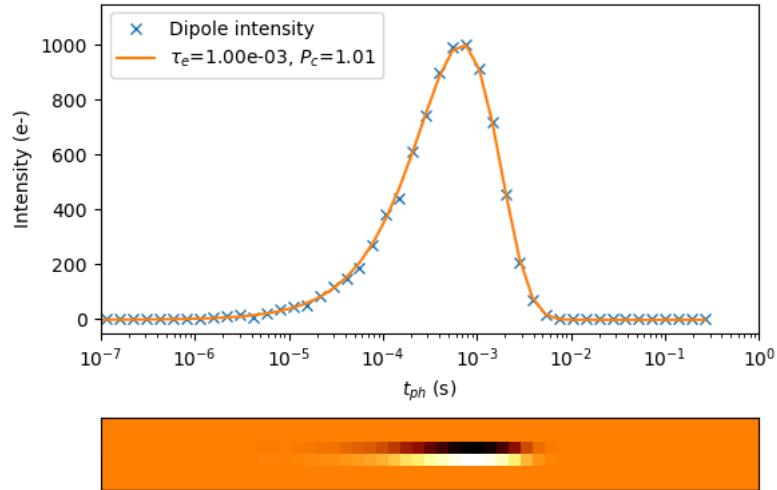
Figure 3. Dipole intensities as a function of phase time T_{ph} values, shown as black and white dipoles (lower panels) and as an intensity curve (upper panel) that is fitted with eq. 2.1 to extract τ_e and P_c. Both plots uses the same t_{ph} values on the x-axis.

2.1 Simulating dipole maps

As part of the Euclid radiation testing campaign performed at the Centre for Electronic Imaging (CEI) at the Open University, the CEI CCD Charge Transfer Model (C3TM) was developed (previously known as OUMC [11]) for simulating Charge Transfer Inefficiency (CTI) in CCDs. C3TM is made to mimic the physical properties in the CCD as closely as possible. To avoid making any analytical assumptions about the size and density of the charge cloud, the model therefore takes device specific simulations of electron density as a direct input.

The actual dipole intensity of a trap depends on a number of things, including the geometry of the pixel and electrodes, the position of the trap in the pixel, the signal size, and the clocking scheme used. All of these parameters can be put into C3TM to simulate the trap pumping scheme, ensuring that the simulations are as close as possible to the laboratory data.

Using C3TM, a trap with a known τ_e value can be inserted at any 3D position in a single row of pixels. By pumping this at a range of t_{ph} values, a figure similar to figure 3 (lower panel) can be obtained. This principle can be used to produce a map of how dipoles will look depending on their position across the pixel. In figure 4 100 traps with the same τ_e value have been inserted in a single row of pixels over a range of sub-pixel positions along the width of the pixel, but with 5 pixels between each trap, such that the first trap is at pixel 5 sub-pixel position 0.005, the next at position 10.010, the next 15.015, etc. The 1-2-3-1'-3-2-1 clocking scheme has been run for that row of pixels at a range of t_{ph} values and each row of pixels therefore represent a single t_{ph} value.

As expected then figure 4 shows that traps under phase 2 will pump charge to the pixel to the left (high-low dipole), traps under phase 3 will pump to the right (low-high dipole) and trap under phase 1 will not pump. It also shows that only parts of phase 2 and 3 will pump and this coincides with the size of the charge cloud [11].
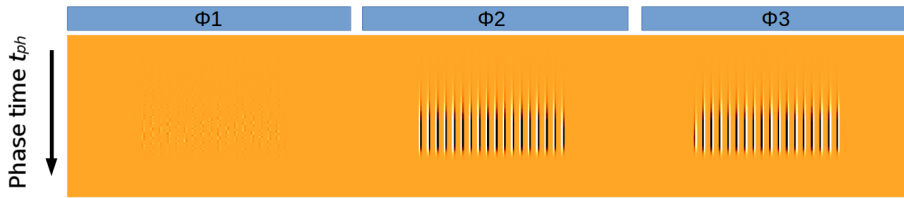

Figure 4. Dipole map of a three-phase device using the standard 1-2-3-1'-3-2-1 clocking scheme, showing that traps under phases 2 and 3 will pump in different directions, and that traps under phase 1 will not pump.

3 Clocking scheme for Euclid

As the CCD273 is a four phase device with uneven electrode widths, an alternative clocking scheme is needed. Using the C3TM software, a number of clocking schemes has been simulated and a few of these has been tested in the lab.

The clocking scheme that was found to be the best is the sub-pixel clocking scheme, which was developed for the P- vs. N-channel CCD irradiation study performed at the CEI [12]. This clocking scheme only moves the charge between three of the four phases in the device. An example of this clocking 1-2-3-2-1, which produces the dipole map shown in figure 5. The dipole map shows that pumping will only occur in the outer half of the end phases, in this case the left hand side of phase 1 and the right hand side of phase 3. As traps under phase 1 will pump to the pixel in the opposite direction of phase 3, the direction of the dipole will tell you under which phase the trap is located. As only traps under half of the phase will pump, it is therefore possible to gain sub-phase positional information about the traps. Further, as figure 5 is made using varying signal sizes, it also gives an idea about how the charge cloud changes with signal size. So by comparing which traps are found at which signal levels, the sub-phase positional information can be improved even further.

The fact that such a small part of the pixel is covered means that four sub-pixel clocking schemes; 1-2-3-2-1, 2-3-4-3-2, 3-4-1'-4-3, and 4-1'-2'-1'-4 (from here on denoted 123, 234, 341', and 41'2', respectively) i.e. one starting in each phase; has to be run in order to cover the whole pixel (see figure 6). This is of course time consuming, but it does come with a benefit; in case there are two or more traps within one or two pixels of each other, there is a risk that these traps can pump against each other and either cancel or distort the dipole. This makes it difficult or impossible to characterise or even identify the traps. As the radiation
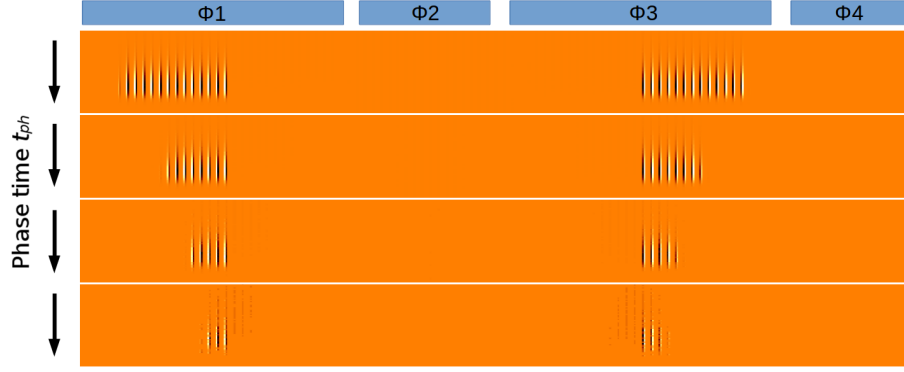
Figure 5. Simulation of the sub-pixel clocking scheme 1-2-3-2-1 (123) at different signal levels, showing the dipole created from a trap .

damage builds up over the mission lifetime, having traps in adjacent pixels becomes more and more likely. However, when only a small part of the pixel is probed, the probability of the traps pumping against each other is also smaller, and the trap pumping results from this scheme should therefore be useful even at high radiation doses.
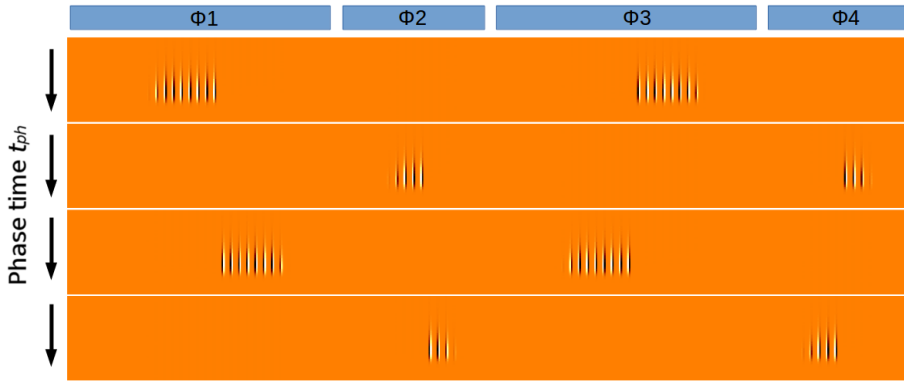

Figure 6. Simulation of the four sub-pixel clocking schemes (from top to bottom: 123, 234, 341', and 41'2') at a signal level of 10,000 e⁻.

4   Results from Pre-irradiated devices

The experimental data for this analysis have been obtained using a pre-irradiated CCD273-EM1A device. The CCD273 is a 4k×4k devices with 4 output nodes, thus giving each node a 2k×2k area. The CCD and its headboard is mounted inside a vacuum chamber that allows the device to be cooled to cryogenic temperatures using a CryoTiger refrigeration system. A small LED inside the vacuum chamber delivers a flatfield signal, however, before any dipole is detected, any pixel-to-pixel non-uniformities or gradients in the flat-field signal is calibrated out. A similar setup is used in [13], where it is also described in more detail.

Each of the four trap pumping schemes are run at a range of logarithmically spaced t_{ph} values between 3 us and 17 ms. This is done at at three temperatures 149 K, 153 K and 157 K, to match the Euclid VIS focal plane operating temperature of 153 K and the expected deviation from this temperature of a few K.

The data are analysed using an automated dipole identification routine, and the dipole intensities are fitted using eq. 2.1, to find the τ_e value for each trap. Figure 7 shows a histogram of the τ_e values found on a single node of the CCD273 device using the 123 clocking scheme at the three different temperatures.
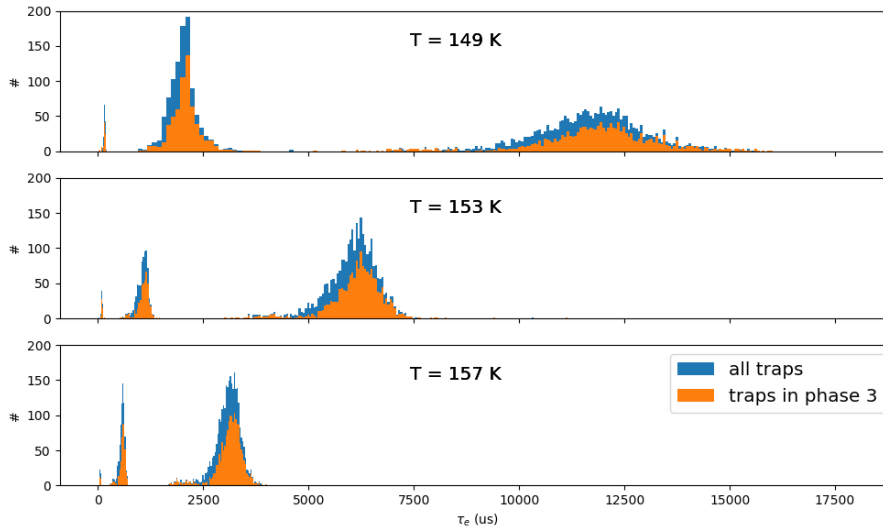
Figure 7. Histogram of τ_e values using the 123 clocking scheme at 1600 e⁻ and at three temperatures: (top to bottom) 149 K, 153 K and 157 K.

By fitting each of the peaks with a gaussian function, the mean τ_e values can be found. Plotting these against temperature, see figure 8, shows that they follow the same trends as previously detected species. The τ_e peaks matches defects from Phosphorus and Boron, which is used as dopants in the CCD manufacturing process, mixed with Carbon and Oxygen impurities that is naturally occurring in the silicon wafers [14]. As these are data from an un-irradiated device the densities are very low, especially for the vacancy-based species emphasised in the legend of figure 8 that are not detectable in these data. However, after irradiation we believe that the vacancy based defects will become dominant.

5 Electrode widths

The design widths of the four parallel electrodes on the CCD273 are 4-2-4-2 μm, however, this does not take the spacing between the electrodes into account. Up until this point all simulations therefore assume 3.5-2-3.5-2 μm electrodes, with a 0.25 μm spacing between each pair of electrodes.

The histograms of all four pumping schemes at 153 K are plotted in figure 9 (left). This shows that almost no traps are found by the 234 scheme, and that scheme 41'2' detects more than twice as many traps as schemes 123 and 341'. This is contrary to the predictions that as electrodes 2 and 4 are about half as wide as electrodes 1 and 3, schemes 234 and 41'2' would detect about half as many traps as 123 and 341', as also indicated by figure 6. This prediction is supported by figure 9 (left), where the four clocking schemes are simulated with C3TM using the 3.5-2-3.5-2 μm electrode widths.

One possible explanation for this could be that the electrode widths are slightly different than expected. If, for instance, electrode 1 is 4 μm and electrode 3 is 3 μm, then the symmetry of the schemes would change and much fewer traps would pump in the 234 scheme. This situation is simulated and the resulting histogram plotted in figure 10 (left). This shows that much fewer traps are indeed detected in the 234 scheme, but more traps are not detected in the 41'2' scheme as are the case in laboratory data in figure 9 (left).

Figure 10 (right) shows the resulting histograms from a simulation where the electrode widths are 3.5-2.5-2.5-2.5 μm, i.e. that phases 2-4 are the same size, and phase 1 is slightly bigger. In this situation the ratio of traps detected between the four schemes is much closer to the laboratory data; schemes 123 and 341' detects similar amounts of traps, while scheme detects 234 very few traps. Scheme 41'2' detects more traps
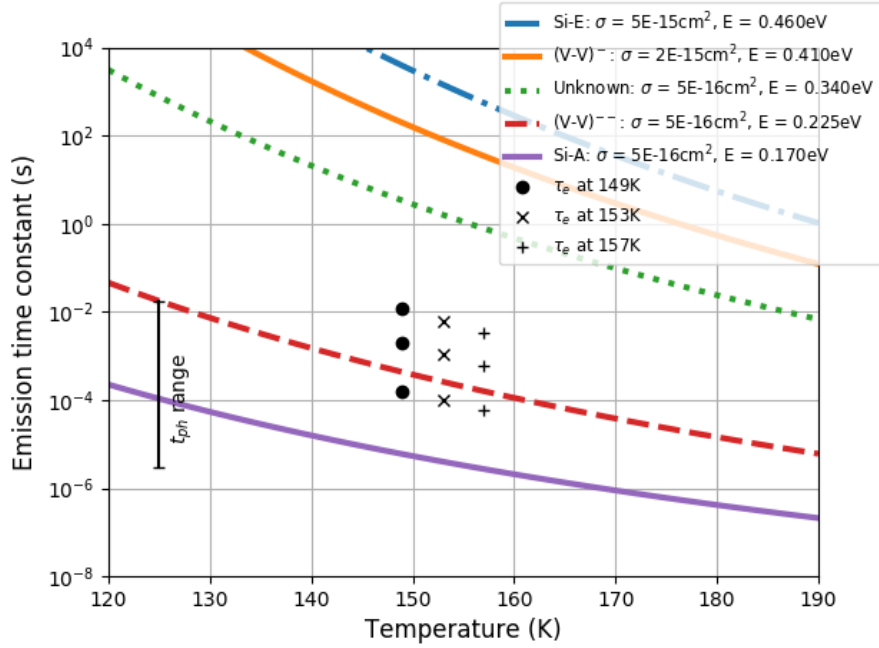
Figure 8. Emission time constants of different well-known defects as a function of temperature. The three peaks from the trap pumping data is shown as dots, x'es and plusses for 149 K, 153 K and 157 K, respectively. The vertical bar at 125 K shows the range of t_{ph} values used in these trap pumping tests.

than the two former schemes, but only about 1.6 times more, not the 2-2.5 times more that is the case in the laboratory data.

Another test of the electrode sizes is to measure the Full Well Capacity (FWC) of the single electrodes. This measurement where made during the laboratory testing of the device and the results are summarized in table 1. These support the claim that electrode 1 is bigger than electrode 3, but they also indicate that electrode 3 is somewhat bigger than electrodes 2 and 4, which slightly contradicts the simulation results.

**Table 1**. Full Well Capacity measurements of the single electrodes.

	Electrode 1	Electrode 2	Electrode 3	Electrode 4
FWC (e^-)	~ 190, 000	~ 110, 000	~ 150, 000	~ 100, 000

By doing more simulations with varying electrodes widths it may be possible to find a solution that matches both the trap pumping and FWC data. So, although the results are not conclusive at this point, it does seem that the sub-pixel trap pumping scheme can be used to gain more information about the effective widths of the parallel electrodes.

6 Conclusion

The trap pumping method will be part of the in-orbit calibration routines for the Euclid VIS instrument, in order to help in the mitigation of the damage of the CCD detectors caused by the harsh radiation environment in space. A number of different trap pumping schemes have been tested and the sub-pixels clocking scheme has been chosen for the image region of the Euclid CCD273 devices.

It is shown that besides giving information about emission time constant and capture probability for the single traps, this clocking scheme is also able to give sub-pixel and even sub-phase positional information.
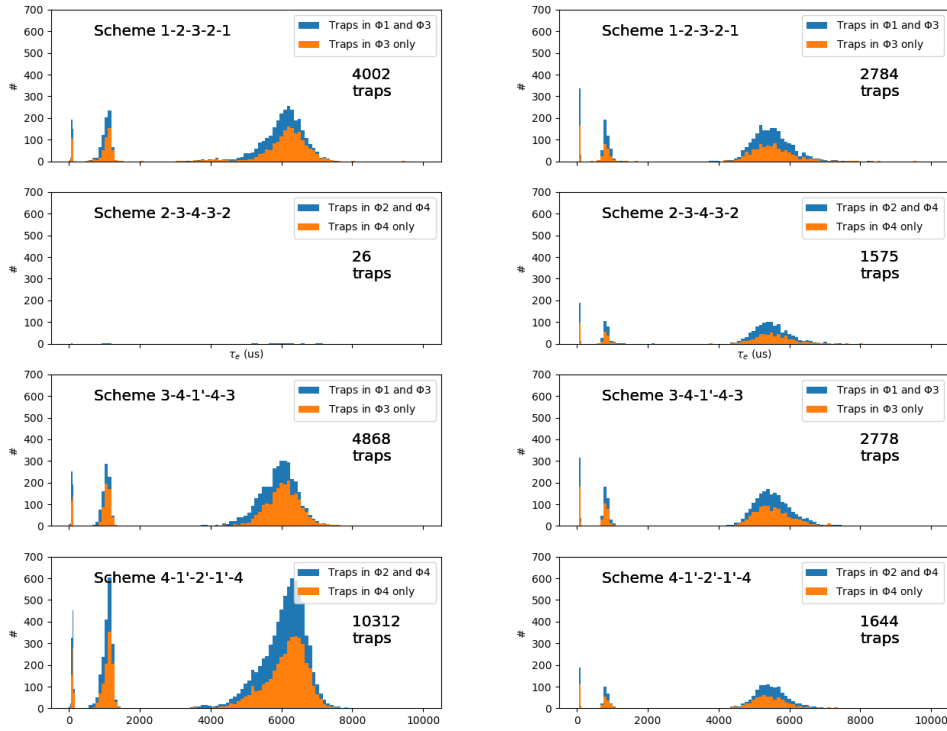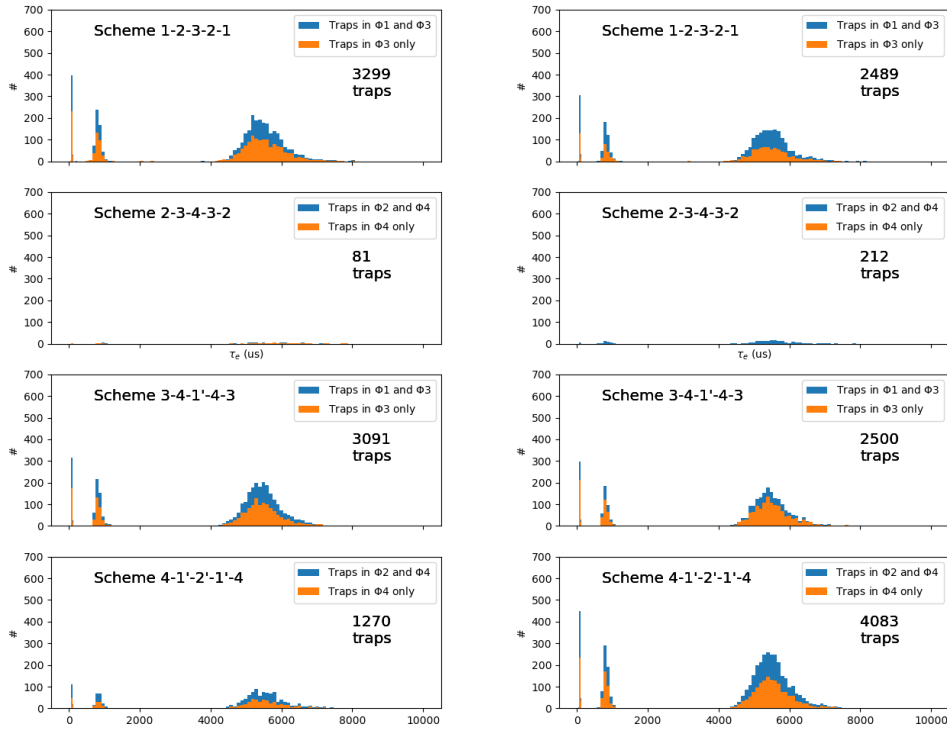
Figure 9. Histograms of all four pumping schemes at 153 K for (left) laboratory data and (right) simulated data using 3.5-2-3.5-2 µm electrode widths with 0.25 µm spacing between the electrodes.

A number of un-irradiated devices have been tested in the laboratory and the data from these tests reveals defects associated with Phosphorus and Boron dopants mixed with naturally occuring Oxygen and Carbon impurities.

We also find that by comparing laboratory data with simulations, the sub-pixel trap pumping scheme can be used to infer information about the effective widths of the electrodes in the CCD. This appears to indicate that the electrode widths in the parallel register are slightly different than expected. It should be noted, though, that a small uncertainty on the electrode widths will not be an issue for the Euclid mission, as the normal readout mode for the CCD273 is to always have two phases coupled together and the uncertainty on the electrode widths will therefore even out.

References

[1] R. Laureijs, J. Amiaux, S. Arduini, J. . Auguères, J. Brinchmann, R. Cole, M. Cropper, C. Dabin, L. Duvet, A. Ealet, and et al. Euclid Definition Study Report. *ArXiv e-prints*, 1.1, October 2011.

[2] Mark Cropper, S. Pottinger, S. Niemi, R. Azzollini, J. Denniston, M. Szafraniec, S. Awan, Y. Mellier, M. Berthe, J. Martignac, C. Cara, A.-M. Di Giorgio, A. Sciortino, E. Bozzo, L. Genolet, R. Cole, A. Philippon, M. Hailey, T. Hunt, I. Swindells, A. Holland, J. Gow, N. Murray, D. Hall, J. Skottfelt, J. Amiaux, R. Laureijs, G. Racca, J.-C. Salvignol, A. Short, J. Lorenzo Alvarez, T. Kitching, H. Hoekstra, R. Massey, and H. Israel. Vis: the visible imager for euclid. volume 9904 of *Proc. SPIE*, pages 99040Q–99040Q–16, 2016.

[3] T. Maciaszek, A. Ealet, K. Jahnke, E. Prieto, R. Barbier, Y. Mellier, A. Costille, F. Ducret, C. Fabron, J.-L. Gimenez, R. Grange, L. Martin, C. Rossin, T. Pamplona, P. Vola, J. C. Clémens, G. Smadja, J. Amiaux, J. C. Barrière, M. Berthe, A. De Rosa, E. Franceschi, G. Morgante, M. Trifoglio, L. Valenziano, C. Bonoli, F. Bortoletto, M. D'Alessandro, L. Corcione, S. Ligori, B. Garilli, M. Riva, F. Grupp, C. Vogel, F. Hormuth, G. Seidel, S. Wachter, J. J. Diaz, F. Grañena, C. Padilla, R. Toledo, P. B. Lilje, B. G. B. Solheim,

Figure 10. Histograms of all four pumping schemes at 153 K for simulated data using (left) 4-2-3-2 μm electrode and (right) 3.5-2.5-2.5-2.5 μm electrode widths, both with 0.25 μm spacing between the electrodes.

C. Toulouse-Aastrup, M. Andersen, W. Holmes, U. Israelsson, M. Seiffert, C. Weber, A. Waczynski, R. J. Laureijs, G. Racca, J.-C. Salvignol, and P. Strada. Euclid near infrared spectrophotometer instrument concept and first test results at the end of phase B. In *Space Telescopes and Instrumentation 2014: Optical, Infrared, and Millimeter Wave*, volume 9143 of *Proc. SPIE*, page 91430K, August 2014.

[4] R. Massey, T. Schrabback, O. Cordes, O. Marggraf, H. Israel, L. Miller, D. Hall, M. Cropper, T. Prod'homme, and S.-M. Niemi. An improved model of charge transfer inefficiency and correction algorithm for the Hubble Space Telescope. *MNRAS*, 439:887–907, March 2014.

[5] H. Israel, R. Massey, T. Prod'homme, M. Cropper, O. Cordes, J. Gow, R. Kohley, O. Marggraf, S. Niemi, J. Rhodes, A. Short, and P. Verhoeve. How well can charge transfer inefficiency be corrected? A parameter sensitivity study for iterative correction. *MNRAS*, 453:561–580, October 2015.

[6] J. R. Janesick. *Scientific charge-coupled devices*. SPIE-Intl Soc Optical Eng, 2001.

[7] R. Kohley, F. Raison, and J. M. Martin-Fleitas. Gaia: operational aspects and tests of Gaia Flight Model CCDs. In *Astronomical and Space Optical Systems*, volume 7439 of *Proc. SPIE*, page 74390F, August 2009.

[8] N. J. Mostek, C. J. Bebek, A. Karcher, W. F. Kolbe, N. A. Roe, and J. Thacker. Charge trap identification for proton-irradiated p+ channel CCDs. In *High Energy, Optical, and Infrared Detectors for Astronomy IV*, volume 7742 of *Proc. SPIE*, page 774216, July 2010.

[9] N. J. Murray, A. D. Holland, J. P. D. Gow, D. J. Hall, J. H. Tutt, D. Burt, and J. Endicott. Mitigating radiation-induced charge transfer inefficiency in full-frame CCD applications by 'pumping' traps. In *High Energy, Optical, and Infrared Detectors for Astronomy V*, volume 8453 of *Proc. SPIE*, page 845317, July 2012.

[10] D. J. Hall, N. J. Murray, A. D. Holland, J. Gow, A. Clarke, and D. Burt. Determination of In Situ Trap Properties in CCDs Using a "Single-Trap Pumping" Technique. *IEEE Transactions on Nuclear Science*, 61:1826–1833, August 2014.

[11] Jesper Skottfelt, David J. Hall, Jason P. D. Gow, Neil J. Murray, Andrew D. Holland, and Thibaut Prod'homme. Comparing simulations and test data of a radiation damaged charge-coupled device for the euclid mission. *Journal of Astronomical Telescopes, Instruments, and Systems*, 3(2):028001, 2017.

[12] Nathan Bush, Ben Dryer, Anton Lindley DeCaire, Ross Burgon, and Andrew Holland. A comparison of proton damage effects on P- and N-Channel CCDs I: Performance following cryogenic irradiation. *In prep.*, 2017.

[13] J. P. D. Gow, N. J. Murray, D. J. Hall, A. S. Clarke, D. Burt, J. Endicott, and A. D. Holland. Assessment of proton radiation-induced charge transfer inefficiency in the CCD273 detector for the Euclid Dark Energy Mission. In *High Energy, Optical, and Infrared Detectors for Astronomy V*, volume 8453 of *Proc. SPIE*, page 845316, July 2012.

[14] Peter Pichler. *Intrinsic Point Defects, Impurities, and Their Diffusion in Silicon*. Computational Microelectronics. Springer-Verlag Wien, 2004.